

Effects of high-pressure hydrogen charging on the structure of austenitic stainless steels

M. Hoelzel^{a,*}, S.A. Danilkin^b, H. Ehrenberg^a, D.M. Toebbens^b,
T.J. Udoovic^c, H. Fuess^a, H. Wipf^d

^a Institute for Materials Science, Darmstadt University of Technology, Petersenstrasse 23, 64287 Darmstadt, Germany

^b Hahn-Meitner-Institut, SF2, Glienicker Str. 100, 14109 Berlin, Germany

^c NIST Center for Neutron Research, National Institute of Standards and Technology, 100 Bureau Drive, MS 8562, Gaithersburg, MD 20899-8562, USA

^d Darmstadt University of Technology, Institute for Solid State Physics, Hochschulstrasse 6, 64289 Darmstadt, Germany

Received 22 January 2004; received in revised form 2 June 2004

Abstract

The effects of high-pressure hydrogen and deuterium charging on the structure of AISI type 304 and AISI type 310 austenitic stainless steels have been investigated by neutron and X-ray diffraction. Rietveld analyses of the neutron diffraction data revealed that hydrogen atoms occupy exclusively the octahedral interstitial sites in both steels. No phase transformations have been observed in 310 stainless steel within the whole range of hydrogen-to-metal atomic ratios H/Me up to ≈ 1 . In 304 stainless steel, the formation of ϵ -martensite was observed not only after hydrogenation at 3.0 GPa (H/Me = 0.56), but also after applying a pressure of 4.0 GPa without hydrogen. The results differ significantly from published studies on cathodically hydrogenated samples, where high amounts of ϵ -martensite were observed in both steels. High-pressure hydrogenation and cathodic hydrogen charging result in different phase transformation behaviour. The discrepancies can be explained by different hydrogen distributions resulting in quite different stress states.

© 2004 Elsevier B.V. All rights reserved.

Keywords: Neutron diffraction; Austenitic stainless steels; Hydrides; Martensitic phase transformation; Hydrogen embrittlement

1. Introduction

The formation of brittle martensite or hydride phases, as a possible source for hydrogen embrittlement, has been discussed extensively. X-ray diffraction studies on cathodically hydrogen-charged austenitic stainless steels have been performed to investigate possible phase transformations due to hydrogen loading [1–10]. The austenitic stainless steels of AISI type 304 (composition close to Fe/Cr18/Ni10) and AISI type 310 (composition close to Fe/Cr25/Ni20) have been studied most extensively in this context. Both steels do not transform to martensites by quenching to liquid nitrogen temperature. 304 stainless steel is a “metastable” steel, which

may form martensite phases as a result of severe plastic deformation, whereas 310 stainless steel is a “stable” steel, which does not undergo any stress- or strain-induced martensitic transformations.

In numerous studies, the formation of hcp ϵ -martensite in 304- and 310-type austenitic stainless steels was observed as a result of hydrogen charging [3–8]. It was also reported that bcc α -martensite is formed during the outgassing of hydrogen from 304 stainless steel, whereas no α -martensite was detected in 310 stainless steel [7]. Some controversy exists about a possible fcc γ^* -hydride phase as precipitates in the austenite lattice as proposed by Narita et al. [7] and Ulmer et al. [8]. Their proposed pseudo-binary phase diagram of the austenite–hydrogen system (referred to both steel compositions) includes a miscibility gap—similar to the palladium–hydrogen [11] and nickel–hydrogen [12] systems. However, Mathias et al. [3] and Gavriljuk et al. [6]

* Corresponding author. Tel.: +49-089-289-14314;
fax: +49-089-289-14666.

E-mail address: Markus.Hoelzel@frm2.tum.de (M. Hoelzel).

observed a continuous expansion of the austenite lattice due to hydrogen charging of 304 and 310 stainless steels, without any miscibility gap in the austenite–hydrogen phase diagram.

In most studies, the hydrogenation has been carried out by cathodic charging at room temperature. This procedure induces a very high hydrogen concentration at the surface followed by a steep gradient. The inhomogeneous hydrogen distribution results in high multiaxial compressive stresses at the surface [7]. The mutual influence of intrinsic effects of hydrogen or of high stresses at the surface is therefore under debate.

As an intrinsic effect the decrease of stacking fault energy of austenitic stainless steels has been reported [13]. The $\gamma \rightarrow \varepsilon$ transformation might be related to the formation of stacking faults on the {1 1 1} planes of the austenite lattice [6]. Furthermore, hydrogen could raise the martensitic start temperature (M_s) and the highest temperature for deformation-induced martensite transformation (M_d) [7].

The important impact of high-stresses on the observed phase transformations in austenitic stainless steel has already been discussed by Tahtinen et al. [14], Rozenak et al. [9,10] and Yang et al. [15]. Based on the broadening of X-ray reflections of cathodically charged 316-type stainless steel, stresses of about 5 GPa have been estimated [9]. The formation of ε -martensite, due to cathodic hydrogen charging, appears to be a result of the combined influence of intrinsic effects of hydrogen together with local stresses [15]. Both effects supposedly contribute to the driving force required for the $\gamma \rightarrow \varepsilon$ phase transformation. The outgassing of hydrogen from 304 stainless steel during aging at room temperature is accompanied by the formation of α -martensite as well as the formation of surface cracks [7,15]. Both effects are described as due to high tensile stresses after hydrogen losses [15].

In order to achieve quite homogeneous hydrogen distributions in the bulk of the samples, we performed hydrogenations of 304 and 310 stainless steels in a high-pressure cell. Homogeneous samples allow a better identification of possible hydride phases and the study of hydrogen effects in a rather low-stress state. Results from different charging techniques enable a comparison of the conditions of phase transformations by hydrogen loadings with respect to hydrogen contents and stresses. Moreover, the hydrogenation of the bulk allows neutron diffraction investigation of the hydrogen locations and occupancies. Simultaneously, inelastic neutron scattering was performed to characterize the interatomic bonding and to get complementary information about the phase composition. In this work, results of the structural analysis by neutron and X-ray diffraction are reported.

2. Experimental

The investigations were performed on commercial AISI type 304 and AISI type 310 austenitic stainless steels. The

hydrogenations have been carried out in the Institute of Solid State Physics of the Russian Academy of Sciences in Chernogolovka (Moscow district). The samples consisted of stacks of 3–6 discs, each of 8 mm diameter and 0.25 mm thickness. The hydrogen loadings were performed in a high-pressure cell at 350 °C for 24 h. Hydrogenation at elevated temperatures for rather long charging times removes concentration gradients due to diffusion. Various pressures, up to 7 GPa, were applied in order to obtain different hydrogen and deuterium concentrations up to H/Me ≈ 1. After the charging, the samples were cooled down to 100 K and stored at liquid nitrogen temperature to prevent the outgassing of hydrogen. More details about the hydrogenation technique can be found in [16]. Additional samples were subjected to 3.0 and 4.0 GPa without hydrogen. These pressure treatments were performed in a high-pressure cell for 24 h at 350 °C in the Institute for Mineralogy at the University of Frankfurt, Germany.

The neutron diffraction experiments were carried out at the multidetector powder diffractometer E9 at the Hahn-Meitner-Institut in Berlin and BT1 at the National Institute of Standards and Technology in Gaithersburg. The measurements at E9 were performed at 80 K using a germanium (7 1 1) monochromator, yielding $\lambda = 1.3078 \text{ \AA}$. At BT1, the data were collected at 80 K using a copper (3 1 1) monochromator and neutrons of $\lambda = 1.5398 \text{ \AA}$.

Additional X-ray diffraction studies were undertaken prior to the hydrogen chargings in the hydrogenated state at 100 K and after hydrogen outgassing at room temperature. A STOE STADI P powder diffractometer in transmission geometry with Mo-K α_1 and Co-K α_1 radiations was used.

3. Results and discussion

The diffraction patterns were analysed by Rietveld refinement with the FullProf software. Figs. 1 and 2 show the measured and calculated diffraction patterns. The main results of the Rietveld refinement are summarized in Tables 1 and 2.

The isotropic thermal displacement parameters of the hydrogen atoms presented in Table 1 and Table 2 were derived from inelastic neutron scattering data, collected at spectrometer FANS at NIST, Gaithersburg. The energies of the fundamental vibrations of the optical modes were used to calculate the mean square displacements $\langle u^2 \rangle$ of the hydrogen atoms. The contribution of hydrogen band modes to the mean square displacements of the hydrogen atoms was neglected at 80 K. The isotropic thermal displacement parameters of hydrogen are related to the mean square displacement $\langle u^2 \rangle$ of the hydrogen atoms by:

$$B_{\text{iso}} = \frac{8\pi^2}{3} \langle u^2 \rangle. \quad (1)$$

The isotropic thermal displacement parameters were kept constant in the Rietveld refinement to obtain the hydrogen occupancies presented in Tables 1 and 2. A refinement of the

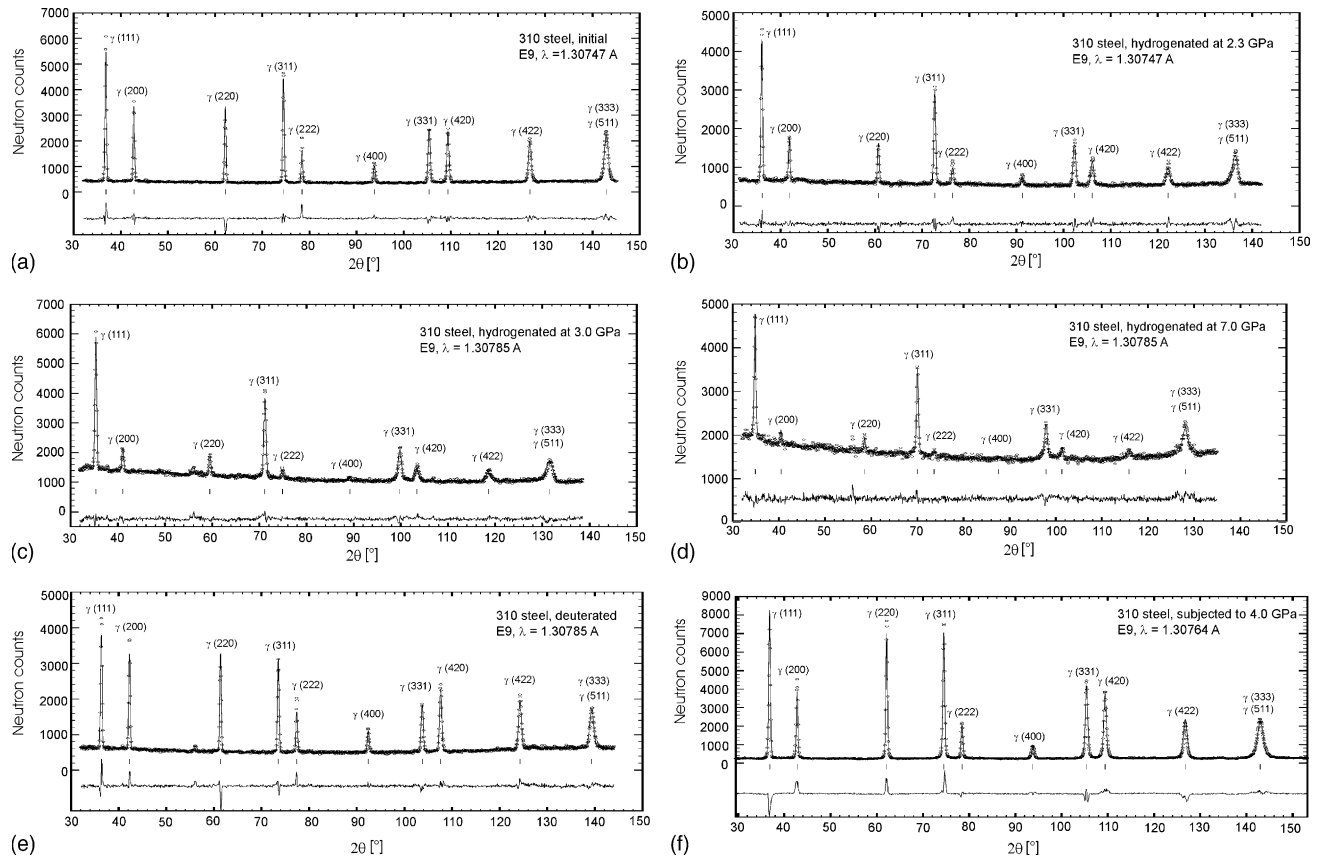


Fig. 1. Measured (circles) and calculated (lines) neutron diffraction patterns as well as difference plots (measured minus calculated diffraction patterns) for 310 stainless steel (Fe/Cr25/Ni20): (a) initial state, (b) hydrogenated at 2.3 GPa, (c) hydrogenated at 3.0 GPa, (d) hydrogenated at 7.0 GPa, (e) deuterated and (f) subjected to 4.0 GPa without hydrogen.

thermal displacement parameters, as a check of the procedure, did not diverge.

3.1. Hydrogen sites

An increasing hydrogenation pressure (i.e., increasing hydrogen content) increases the intensity of the odd-indexed reflections of the austenite phase relative to the even ones (see Figs. 1 and 2 and Tables 1 and 2). This corresponds to hydrogen occupation of the octahedral interstitial sites in the fcc lattice based on structure factor calculations and simulations of diffraction patterns. The opposite effect on the reflection intensities occurred for deuterium charging, due to

the positive neutron scattering length for deuterium ($b_D = +6.67 \cdot 10^{-15}$ m) in contrast to the negative one for hydrogen ($b_H = -3.74 \cdot 10^{-15}$ m). Finally, Rietveld refinement proved hydrogen (deuterium) occupation of the octahedral interstitial sites in the fcc matrices only. No occupation of the tetrahedral sites for all investigated hydrogen concentrations in both steels was detected.

The occupancy in the octahedral sites in austenitic stainless steels corresponds to the hydrides of iron, nickel and chromium: neutron diffraction investigations on ϵ' -FeH_{1.0}(P6₃/mmc, dhcp lattice) [17], ϵ' -FeD_{1.0}(P6₃/mmc, dhcp lattice) [17], ϵ -FeD_{0.42}(P6₃/mmc, dhcp lattice) [17], ϵ -CrH_{≈1}(P6₃/mmc, hcp lattice) [18] and NiH_{0.6}(Fm3m) [12]

Table 1
Results of the Rietveld analyses of 310 stainless steel (Fe/Cr25/Ni20)

Hydrogenation pressure (GPa)	Sample mass (g)	Weight fractions of phases	Lattice constant (at 80 K)	H-occupancy in octahedral sites (%)	Thermal displacement parameter B_{iso} (H) (Å ²)
Uncharged	0.6	100% Fm $\bar{3}m$	3.5826(1)	—	—
2.3	0.6	100% Fm $\bar{3}m$	3.6586(1)	35(2)	1.35
3.0	0.6	100% Fm $\bar{3}m$	3.7261(2)	66(3)	1.44
7.0	0.3	100% Fm $\bar{3}m$	3.7798(2)	94(5)	1.48
Deuterium ^a	0.3	100% Fm $\bar{3}m$	3.6236(1)	13(1)	0.96
4.0 Without H	0.8	100% Fm $\bar{3}m$	3.5824(2)	—	—

^a For deuterium charging, the true charging pressure is unclear.

Table 2
Results of the Rietveld analyses of 304 stainless steel (Fe/Cr18/Ni10)

Hydrogenation pressure (GPa)	Sample mass (g)	Weight fractions of phases	Lattice constant (at 80 K)	H-occupancy in octahedral sites (%)	Thermal displacement parameter B_{iso} (H) (\AA^2)
Uncharged	0.6	100% $Fm\bar{3}m$	3.5800(1)		
2.3	0.6	100% $Fm\bar{3}m$	$a = 3.6537(1)$	30(2)	1.39
3.0	0.6	84% $Fm\bar{3}m$ 16% $P6_3/mmc$	fcc: $a = 3.6988(2)$ hcp: $a = 2.617(2); c = 4.254(3) c/a = 1.626$	56(2) 71(9)	1.41
7.0	0.3	Not analysed	fcc: $a = 3.7757(3)$	103(9)	1.48
4.0 Without H	1.2	86% $Fm\bar{3}m$ 11% $P6_3/mmc$ 3% $Im\bar{3}m$	fcc: $a = 3.5785(2)$ hcp: $a = 2.526(1); c = 4.098(4) c/a = 1.622$ bcc: $a = 2.8571(3)$		

revealed in all cases an occupancy of the octahedral interstitial positions. This has been proposed for the hydrides of transition metals of the groups VIb–VIIIb [17,19]. Because of the small size of the interstices in the lattices of these elements, hydrogen occupies the bigger octahedral sites only in fcc and hcp hydrides.

3.2. Phase analysis

The hydrogenation of 310 stainless steel leads to a continuous expansion of the austenite lattice. No significant reflections other than fcc appeared in the diffraction patterns. This was further confirmed by X-ray diffraction at 100 K. The small reflection in the vicinity of the γ -(220) reflection (Fig. 1c–e) was also observed in a pattern of the empty vanadium sample holder and thus does not correspond to scattering from the samples. Our results differ significantly from results obtained by cathodic hydrogenation, where quite strong reflections of ϵ -martensite were observed [3–7].

Vakhney et al. [20] calculated the total energy and electron density-of-states at the Fermi energy of the γ -phase and ϵ -phase in 310 stainless steel for H/Me atomic ratios of 0, 0.5 and 1. They proposed the ϵ -phase as stable at around H/Me = 0.5. The $\gamma \rightarrow \epsilon$ transformation was supposed to result from the influence of hydrogen on the electronic structure of 310 stainless steel. Since we do not observe reflections of the ϵ -phase for H/Me up to ≈ 1 in the bulk of 310 stainless steel within the detection limit, our results do not support this hypothesis.

In 304 stainless steel, a different phase transformation behaviour was observed (Fig. 2 and Table 2). The sample hydrogenated at 2.3 GPa, consists of a pure expanded fcc lattice, whereas for the sample hydrogen-charged at 3.0 GPa (H/Me = 0.56) reflections of ϵ -martensite appear. The weight fraction of ϵ -martensite was refined to 16 wt.%. The formation of ϵ -martensite was also detected in the sample of 304 stainless steel, which had been squeezed at 4.0 GPa with-

out hydrogen with a weight fraction of 11 wt.%. In addition, a small amount (≈ 3 wt.%) of bcc α -martensite was also observed.

In the studies on cathodically charged 304 and 310 stainless steels, generally very intense X-ray reflections of ϵ -martensite have been reported [3–7]. Based on an empirical relation between the lattice expansion and the hydrogen contents of fcc alloys [21], hydrogen contents of H/Me ≈ 0.6 have been estimated for cathodically charged austenitic stainless steels [20,22]. Farrell et al. [23] evaluated depth concentration profiles from nuclear microanalysis of 310 stainless steel cathodically charged with deuterium: D/Me atomic ratios between 0.5 and 0.8 have been found in the near-surface layers. Based on the hydrogen contents, one can compare the results obtained after high-pressure hydrogenation and electrolytic charging: the cathodic charging technique leads to higher amounts of ϵ -martensite at comparable hydrogen contents. In 310 stainless steel, ϵ -martensite was not observed within the detection limit even after high-pressure charging.

Remarkable differences in the phase transformation behaviour, as a result of electrolytic or high-pressure hydrogenation of austenitic steels, were also observed by Bugaev et al. [22]. High-pressure charging at 7 GPa and 200 °C was performed on fcc Fe–18Cr–16Ni–10Mn, for which a very high stability of the austenite phase is claimed due to the high contents of manganese and nickel. X-ray diffraction disclosed that no phase transformations took place during hydrogenation. A hydrogen content of H/Me = 0.6 has been estimated from the lattice expansion applying the relationship of Baranowski et al. [21]. The lattice expansion matched quite well with the results obtained earlier by cathodic hydrogenation of the same alloy [6], but in case of cathodic charging, strong reflections of ϵ -martensite were observed.

Our data underline the considerable influence of stresses on the phase transformation behaviour of steels subjected to hydrogen chargings. High stresses, arising from inhomogeneous hydrogen distributions in cathodically charged

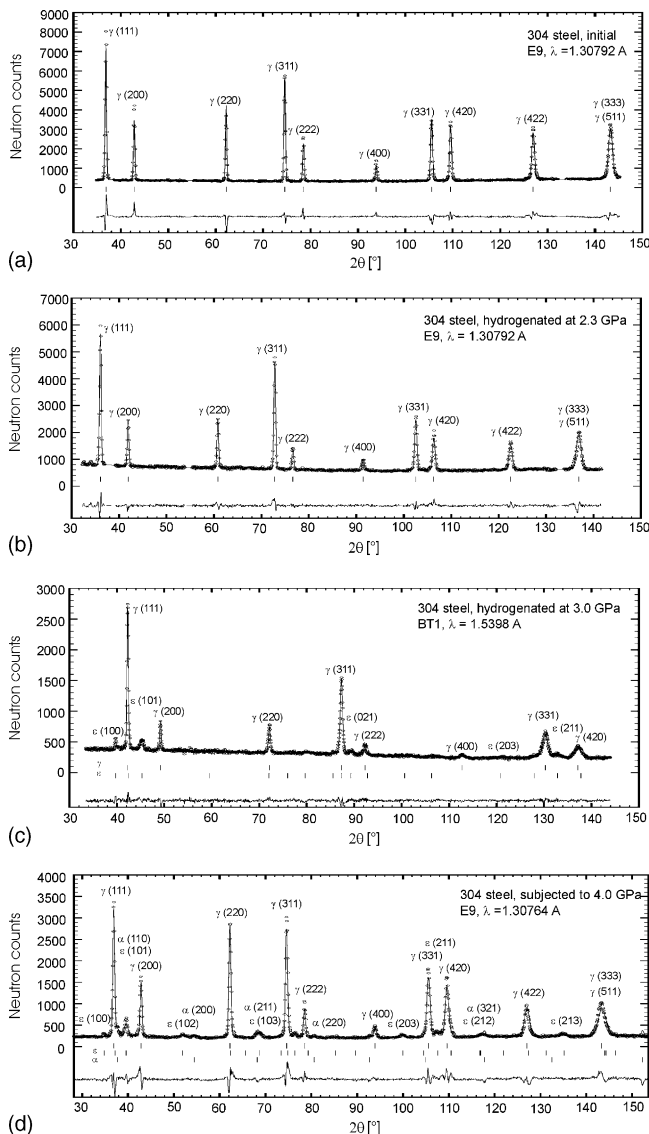


Fig. 2. Measured (circles) and calculated (lines) neutron diffraction patterns as well as difference plots (measured minus calculated diffraction patterns) for 304 stainless steel (Fe/Cr18/Ni10): (a) initial state, (b) hydrogenated at 2.3 GPa, (c) hydrogenated at 3.0 GPa and (d) subjected to 4.0 GPa without hydrogen.

samples, are supposedly responsible for a higher tendency of the ε -martensite formation.

High-pressure hydrogenations result in quite uniform hydrogen distributions and therefore lower stress states compared to cathodic chargings. In 304 stainless steel, similar weight fractions of ε -martensite have been detected after hydrogenation at 3.0 GPa and after a pressure treatment of 4.0 GPa in the absence of hydrogen. The results demonstrate that the impact of stresses has to be considered in the discussion of phase transformations due to hydrogenation.

3.3. Volume increase due to hydrogen

The correlation between the lattice expansion in a single phase due to hydrogen charging and its hydrogen content can

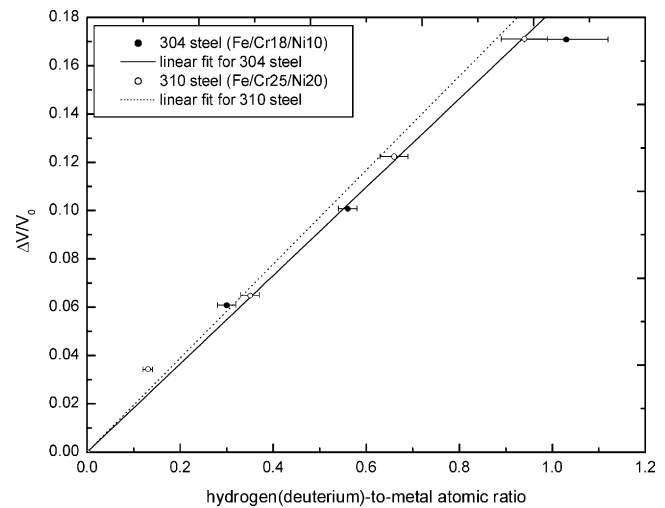


Fig. 3. Lattice expansion vs. H/Me atomic ratio. The slope of the linear fit provides the relative volume changes $\Delta\nu/\Omega$ due to hydrogen.

be described by the following linear relationship [24]:

$$\frac{\Delta V}{V_0} = c_H \frac{\Delta\nu}{\Omega} \quad (2)$$

where $\Delta V/V_0$ is the relative volume change of the unit cell, c_H is the H/Me atomic ratio, $\Delta\nu$ is the volume change of the lattice if one hydrogen atom is added and Ω is the mean atomic volume of a metal atom. Plotting $\Delta V/V_0$ over c_H provides the ratio $\Delta\nu/\Omega$. Fig. 3 shows this plot for hydrogen in the austenite phase in both steels derived from the Rietveld analyses. Relative volume changes $\Delta\nu/\Omega$ due to hydrogen of 0.18 ± 0.03 for 304 stainless steel and 0.20 ± 0.03 for 310 stainless steel have been derived. Ulmer et al. [8] presented the analogous study for 304 and 310 stainless steels cathodically hydrogenated at elevated temperatures. In their work, similar values for $\Delta\nu/\Omega$ of 0.189 for 304 stainless steel and 0.20 ± 0.005 for 310 stainless steel were found. The volume increase per hydrogen atom can be derived directly from the ratio $\Delta\nu/\Omega$. The obtained values of $2.10 \pm 0.01 \text{ \AA}^3$ for 304 stainless steel and $2.24 \pm 0.01 \text{ \AA}^3$ for 310 stainless steel are close to the value of 2 \AA^3 estimated for hydrogen in hexagonal cobalt hydrides and deuterides [25].

3.4. Hydrogen-induced magnetism

Samples of both compositions became ferromagnetic after hydrogenation at 3.0 and 7.0 GPa whereas the samples of lower content still remained paramagnetic at liquid nitrogen temperature. SQUID measurements were carried out on 310 stainless steel hydrogenated at 3.0 GPa. A superconducting quantum interference device from Quantum Design was used to obtain the temperature dependence of the magnetisation at 0.1 T. Fig. 4 illustrates the temperature dependence of the spontaneous magnetisation per iron atom. An unusual linear behaviour is observed in the whole range of the experiment, from 10 to 200 K; the slope corresponds to $-0.001 \mu_B/K$. The

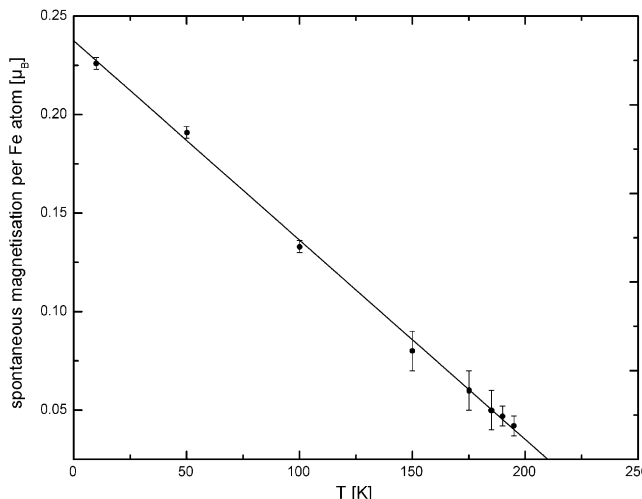


Fig. 4. Temperature dependence of the spontaneous magnetisation found in 310 stainless steel, hydrogenated at 3 GPa, obtained in SQUID measurements at 0.1 T.

temperature dependence of the magnetisation and its inverse can be seen in Fig. 5. The plot of the inverse magnetisation shows a remarkable monotonous behaviour without a definite transition point between the paramagnetic and ferromagnetic regimes. The data points between 236 and 280 K were taken into account to obtain the Curie–Weiss fit of the paramagnetic regime, from which a paramagnetic moment of about $2.5 \mu_B$ per iron atom and a Weiss temperature of about 170–175 K were evaluated. The magnetic contributions to the nuclear Bragg intensities can be neglected in the Rietveld analyses because of the very low ferromagnetic components (see Fig. 4). A possible explanation of the ferromagnetism is the observed lattice expansion. In this context, it is worth noting that properties of hard magnetic materials (SmCo_5 , R_2T_{17} with R = rare earth element; T = Fe, Co) can be varied systematically by hydrogen insertion [26]. In the R_2Fe_{17} series, dramatic increases of the Curie-temperature (by about

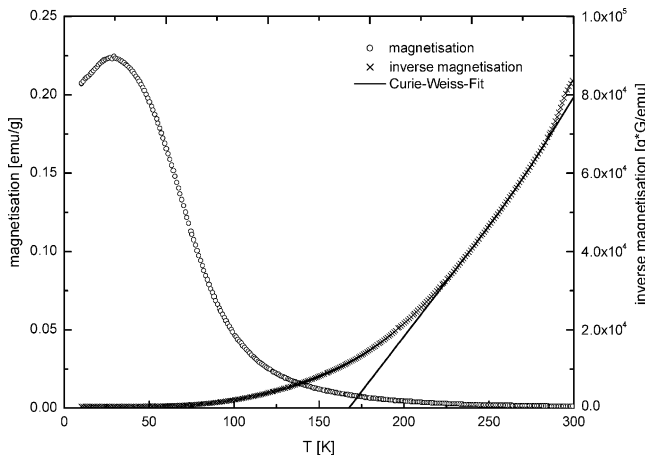


Fig. 5. Temperature dependence of magnetisation and inverse magnetisation in stainless steel 310, hydrogenated at 3.0 GPa, obtained in SQUID measurements at 0.1 T.

150–200 K) have been achieved. Hydrogenation leads to lattice expansion i.e., the Fe–Fe distance is increased, which strongly influences the magnetic interactions.

4. Conclusion

- (1) Rietveld analyses verified that hydrogen atoms occupy the octahedral interstitial sites in 304 and 310 austenitic stainless steels. A partial occupancy of tetrahedral positions can be ruled out even at $\text{H}/\text{Me} \approx 1$.
- (2) For 310 stainless steel, no phase transformations have been observed within detection limit. For 304 stainless steel, the formation of ϵ -martensite was observed due to hydrogenation at 3.0 GPa, corresponding to a hydrogen content of $\text{H}/\text{Me} = 0.56$. The formation of ϵ -martensite was also found in 304 stainless steel subjected to a pressure of 4.0 GPa without the presence of hydrogen.
- (3) Increasing hydrogen contents lead to continuous lattice expansions of the austenite matrices in both steels. No reflections of a fcc γ^* -hydride phase have been observed for the investigated hydrogen contents.
- (4) The relative volume changes $\Delta V/\Omega$ due to hydrogen charging have been estimated to be 0.20 ± 0.03 in 310 stainless steel and 0.18 ± 0.03 in 304 stainless steel, corresponding to volumes per hydrogen atoms of $2.10 \pm 0.01 \text{ \AA}^3$ for 304 stainless steel and $2.24 \pm 0.01 \text{ \AA}^3$ for 310 stainless steel.
- (5) Both steels become ferromagnetic at high hydrogen contents. In 304 stainless steel, the ferromagnetic ordering occurs between $\text{H}/\text{Me} = 0.30$ and $\text{H}/\text{Me} = 0.56$ and in 310 stainless steel between $\text{H}/\text{Me} = 0.35$ and $\text{H}/\text{Me} = 0.66$.

The high-pressure hydrogenated samples reveal a lower tendency for the ϵ -martensite formation compared to cathodically charged samples, even at hydrogen contents H/Me up to ≈ 1 . The phase transformation behaviour is apparently less determined by the hydrogen concentration rather than the way how hydrogen is introduced into the samples. Cathodic hydrogen chargings lead to higher local stresses due to strong gradients in the hydrogen concentration than high-pressure hydrogenations. The high stresses in cathodic hydrogenated samples can explain a higher driving force for the $\gamma \rightarrow \epsilon$ phase transformation.

Acknowledgements

Financial support from the Bundesministerium für Bildung und Forschung (German Ministry for Education and Science) is gratefully acknowledged. We thank V.E. Antonov and his co-workers from the Institute of Solid State Physics of the Russian Academy of Science in Chernogolovka for their help in the high-pressure hydrogenations. We also thank S. Buhre from the Institute of Mineralogy, University of Frankfurt, for performing high-pressure treatments without hydrogen.

References

- [1] A. Inoue, Y. Hosoya, T. Masumoto, Trans. ISIJ 19 (1979) 170.
- [2] S. Sugiyama, H. Ohkubo, M. Takenaka, K. Ohsawa, M.I. Ansari, N. Tsukada, E. Kuramoto, J. Nuclear Mater. 283–287 (2000) 863.
- [3] H. Mathias, Y. Katz, S. Nadiv, Met. Sci. 12 (1978) 129.
- [4] K.K. Kamachi, Trans. ISIJ 18 (1978) 485.
- [5] A. Szummer, A. Janko, Corrosion 35 (10) (1979) 461.
- [6] V.G. Gavriljuk, H. Hänninen, A.S. Tereshchenko, K. Ullakko, Scripta Metall. et Mater. 28 (1993) 247.
- [7] N. Narita, C.J. Altstetter, H.K. Birnbaum, Met. Trans. A 13A (1982) 1355.
- [8] D.G. Ulmer, C.J. Altstetter, Acta Met. Mater. 41 (7) (1993) 2235.
- [9] P. Rozenak, L. Zevin, D. Eliezer, J. Mater. Sci. Lett. 2 (1983) 63.
- [10] P. Rozenak, D. Eliezer, Acta Metall. 35 (9) (1987) 2329.
- [11] J.E. Worsham, M.K. Wilkinson, C.G. Shull, J. Phys. Chem. Solids 3 (1957) 303.
- [12] E.O. Wollan, J.W. Cable, W.C. Koehler, J. Phys. Chem. Sol. 24 (1963) 1141.
- [13] M.B. Whiteman, A.R. Troiano, Phys. Stat. Sol. 7 (1964) K109.
- [14] S. Tähtinen, P. Nenonen, H. Hänninen, Scripta Metall. 20 (1986) 153.
- [15] Q. Yang, J.L. Luo, Mater. Sci. Eng. A 288 (2000) 75.
- [16] V.E. Antonov, T.E. Antonova, N.A. Chirin, E.G. Ponyatowsky, M. Baier, F.E. Wagner, Scripta Mater. 34 (8) (1996) 1331.
- [17] V.E. Antonov, K. Cornell, V.K. Fedotov, A.I. Kolesnikov, E.G. Ponyatovsky, V.I. Shiryaev, H. Wipf, J. Alloys Comp. 264 (1998) 214.
- [18] G. Albrecht, F.D. Doenitz, K. Kleinstück, M. Betzl, Phys. Stat. Sol. 3 (1963) K249.
- [19] V.A. Somenkov, S.S. Shilstein, Z. Phys. Chem. N.F. 117 (1979) 125.
- [20] A.G. Vakhney, A.N. Yaresko, V.N. Antonov, V.V. Nemoshkalenko, V.G. Gavriljuk, A.V. Tarasenko, I. Smurov, J. Phys.: Cond. Mater. 10 (1998) 6987.
- [21] B. Baranowski, S. Majchrzak, T.B. Flanagan, J. Phys. F: Met. Phys. 1 (1971) 258.
- [22] V.N. Bugaev, V.G. Gavriljuk, Y.N. Petrov, A.V. Tarasenko, Int. J. Hydrogen Energy 22 (2/3) (1997) 213.
- [23] K. Farrell, M.B. Lewis, Scripta Metall. 15 (1981) 661.
- [24] H. Peisl, Hydrogen Met. I, in: G. Alefeld, J. Völkl (Eds.), Topics in Applied Physics, vol. 28, Springer, New York, 1978, pp. 53–74.
- [25] V.K. Fedotov, V.E. Antonov, A.I. Kolesnikov, A.I. Beskrovni, G. Grossse, F.E. Wagner, Sol. State Comm. 107 (12) (1998) 787.
- [26] D. Fruchart, M. Bacmann, P. de Rango, O. Isnard, S. Liesert, S. Miaraglia, S. Obbadé, J.L. Soubeyroux, E. Tomey, P. Wolfers, J. Alloys Comp. 253–254 (1997) 121.